Boundary-Layer Meteorology (2025) 191:12
https://doi.org/10.1007/s10546-025-00901-4

RESEARCH ARTICLE

Scaling the Vertical-Velocity Variance During the Very Late Afternoon Transition of the Convective Boundary Layer

Omar El Guernaoui[1] · **Dan Li**[2] · **Joachim Reuder**[3]

Received: 6 October 2024 / Accepted: 17 January 2025

Abstract

In the bulk of the convective boundary layer driven by surface heating, the vertical-velocity variance is known to scale with the convective velocity scale. This scaling relies on the quasi-equilibrium assumption that the surface heat flux (H, the water-vapor contribution to buoyancy is neglected) varies slowly compared to the adjustment time scale of the large scale convective eddies (or the eddy turnover time), a condition which over land is typically satisfied from the late morning to the early afternoon transition. Later on, when the surface heat flux starts decaying moderately compared to the eddy turnover time, a departure from the quasi-equilibrium regime is expected. A recent idealized large-eddy simulations (LES) study proposed a parameter for describing such departure during the late afternoon transition: $\widetilde{r} \equiv |H^{-1}dH/dt|^{-1}/t_*$, where t_* is the eddy turnover time. The quasi-equilibrium assumption applies when $\widetilde{r} >> 1$, and breaks down when $\widetilde{r} \sim 1$. Building on these results, we further investigate the scaling for the vertical-velocity variance during the very late afternoon transition, i.e. in the regime $\widetilde{r} << 1$ where the surface heat flux decays rapidly compared to the eddy turnover time. In a first step, we use LES to reveal that the regime $\widetilde{r} << 1$ is characterized by a new velocity scale $w_{*r} \equiv ((g/\overline{\theta})|dH/dt|z_i^2)^{1/4}$. Within the specific framework of this study using the parameter $\widetilde{r}$ for identifying the out-of-equilibrium regime $\widetilde{r} << 1$, the proposed scaling is implicitly dependent on the surface heat flux magnitude at the initial state when $\widetilde{r} \approx 0.1$, through the definition of the parameter $\widetilde{r}$. In a second step, we demonstrate that the new velocity scale can be deduced from scaling arguments applied to the budget-equation of the vertical turbulent heat flux.

Keywords Convective boundary layer · Equilibrium breakdown · Large-eddy simulation · Late afternoon transition · Vertical-velocity variance

✉ Omar El Guernaoui
omarelguernaoui@gmail.com

[1] Geophysical Institute, University of Bergen, and Bjerknes Centre for Climate Research, Bergen, Norway

[2] Department of Earth and Environment and Department of Mechanical Engineering, Boston University, Boston, USA

[3] Geophysical Institute and Bergen Offshore Wind Centre, University of Bergen, and Bjerknes Centre for Climate Research, Bergen, Norway

Published online: 07 February 2025

1 Introduction

In the bulk region of the fair-weather convective boundary layer (CBL) located between the surface layer and the interfacial layer, the vertical-velocity variance (σ_w^2) is known to scale with the convective velocity scale $w_* \equiv ((g/\overline{\theta})Hz_i)^{1/3}$ (Deardorff 1970), where g is the acceleration due to gravity, $\overline{\theta}$ is the mean potential temperature of the CBL, H is the surface kinematic heat flux (referred to as surface heat flux hereafter), and z_i is the CBL depth. This scaling applies during strong convective situations when shear production is negligible compared to buoyancy production. In this scaling framework, the vertical-velocity variance is in quasi-equilibrium with the surface heat flux, which can be viewed as the forcing for the CBL. The quasi-equilibrium requires slow variations of the surface heat flux compared to the convective eddy turnover time, a condition which is typically satisfied during a few hours around midday over land (Wyngaard 1973; Kaimal et al. 1976), including the early afternoon transition. However, during the late afternoon transition, the quasi-equilibrium regime breaks down as a result of a moderately or rapidly decaying surface heat flux compared to the convective eddy turnover time. In this study, "the afternoon transition" refers to the stage of the diurnal cycle over land when the surface heat flux gradually decays from its maximum value around midday to zero shortly before sunset (Nadeau et al. 2011).

In a recent idealized LES study, Elguernaoui et al. (2023) (hereafter E23) identified the relevant time scales for characterizing the departure of the free-convective boundary layer from the quasi-equilibrium regime during the late afternoon transition. Both the characteristic time scale of the surface heat flux decay, $\widetilde{\tau}_f(t) \equiv |H^{-1}dH/dt|^{-1}$, and the convective eddy turnover time, $t_*(t) \equiv z_i(t)/w_*(t)$, should be taken into account. During the early afternoon transition when the parameter $\widetilde{r}(t) \equiv \widetilde{\tau}_f(t)/t_*(t)$ is much larger than 1, the quasi-equilibrium assumption is satisfied. The departure starts during the late afternoon transition when the parameter $\widetilde{r}(t)$ approaches 1. Moreover, E23 argued that $w_*(t)$ can still be used to characterize $\sigma_w^2(t)$ when the condition $\widetilde{r} >> 1$ is not satisfied, i.e. despite the breakdown of the quasi-equilibrium relating $\sigma_w^2(t)$ to H through $w_*(t)$. However, when $\widetilde{r} \sim 1$ or $\widetilde{r} << 1$, the functional dependence relating $\sigma_w^2(t)$ to its forcing remains unknown.

This study aims to address this research gap. We use idealized LES of the CBL to show that during the very late afternoon transition when the surface heat flux decays rapidly compared to the convective eddy turnover time, i.e. $\widetilde{r} << 1$, the relevant velocity scale for describing $\sigma_w^2(t)$ is $w_{*r} \equiv ((g/\overline{\theta})|dH/dt|z_i^2)^{1/4}$. Through the definition of the parameter $\widetilde{r}$ involving both the surface heat flux magnitude and its decay rate, the proposed similarity is implicitly constrained by the surface heat flux magnitude at the initial state of the regime $\widetilde{r} << 1$. In order to provide physical arguments supporting the empirical LES results, we carry out a scaling analysis for the budget-equation of the turbulent vertical heat flux. After quantifying the terms in this budget-equation using LES, we show that the transition around $\widetilde{r} \approx 1$ between a quasi-equilibrium regime and an out-of-equilibrium regime corresponds also to a change in the balance among the terms of the heat flux budget. More specifically, the heat-flux tendency term is much smaller than the leading production and destruction terms when $\widetilde{r} >> 1$, while it becomes on the same order of magnitude as the leading terms when $\widetilde{r} << 1$. From the scaling analysis of the heat flux budget, we derive the well-known convective velocity scale w_* and the new velocity scale w_{*r} in the cases where $\widetilde{r} >> 1$ and $\widetilde{r} << 1$, respectively.

2 Numerical Experiments

In this study, we use the PALM model in its LES mode to solve the filtered Navier–Stokes equations within the Boussinesq approximation, together with the filtered budget equation for potential temperature (Maronga et al. 2015). The filtering operation is implicitly achieved by the discretization over a Cartesian C-type staggered grid. We use the second-order advection scheme (Piacsek and Williams 1970) and the third-order Runge–Kutta timestep scheme (Williamson 1980). The SGS terms are parametrized using a 1.5-order flux-gradient scheme after Deardorff (1980). More details about the model can be found in Maronga et al. (2015).

We first derive the new velocity scale from simulations without background wind (free-convection), then we perform an additional set of simulations with prescribed steady background wind (forced-convection). Since Coriolis effects tend to be negligible in turbulence second-moment budgets (Stull 1988; Garratt 1994; Wyngaard 2010), while the scope of this study is limited to scaling the vertical-velocity variance based on the budget of the vertical turbulent heat flux, we neglect Coriolis effects by setting the Earth's rotation to zero. In the hypothetical case where the Coriolis force would had been taken into account in the conservation equations for momentum, the Coriolis term in the budget of the vertical turbulent heat flux would be identically zero (Stull 1988; Wyngaard 2010).

While our study considers the case of a dry atmosphere, Lothon et al. (2014) pointed out that the surface latent heat flux can be comparable to the surface sensible heat flux during the Boundary-Layer Late Afternoon and Sunset Turbulence (BLLAST) field campaign. Note that this is also the case in fair weather over the tropical oceans (Nicholls and Lemone 1980). Thus, from a practical point of view, it is important to consider the effects of moisture on the surface buoyancy flux by using the virtual potential temperature instead of potential temperature. Then, the novel results of our study can be generalized by defining the velocity scale based on the time derivative of the buoyancy flux.

For driving the dry CBL in our simulations, we prescribe a homogeneous surface heat flux. At the bottom boundary, a non-slip condition is imposed. At the top boundary, a free-slip condition is imposed for velocity and potential temperature. For both the perturbation pressure and the SGS-TKE, a zero-gradient Neumann condition is imposed at the bottom and top boundaries. The lateral boundary conditions are cyclic. At the model top boundary, the reflection of gravity waves formed at the interface between the CBL and the free atmosphere can affect the bulk of the CBL. To prevent these effects, a damping layer is added to the upper 100 m of the modelling domain.

At the initial time, the potential temperature equals 300 K at the surface, and increases from there with a rate (λ) of either 3 or 6 K km^{-1} corresponding to the free-atmospheric lapse rate after the CBL development during the spin-up time. These values are typical for fair-weather conditions in the CBL (e.g. André et al. 1978; LeMone et al. 2000; Lothon et al. 2014). The equivalent Brunt–Väisälä frequencies range approximately between 0.01 s^{-1} and 0.014 s^{-1}. In order to trigger the onset of convection during the initial times, random perturbations following a uniform distribution are imposed to the surface heat flux field and to the horizontal-velocity field in the vertical range extending from the near-surface up to a height of one third of the domain height. Starting from this arbitrary initial state, a spin-up time of 3-h physical time (about $18t_*$) is sufficient for reaching a state of statistical equilibrium where the outputs are representative of the modeled system. For example, the spin-up time is about $6t_*$ and $15t_*$ in Moeng and Sullivan (1994) and Salesky et al. (2017) respectively.

Increasing the confidence in the results of this scaling study is dependent on considering a large parameter space, where the governing parameters vary over a broad range of realistic

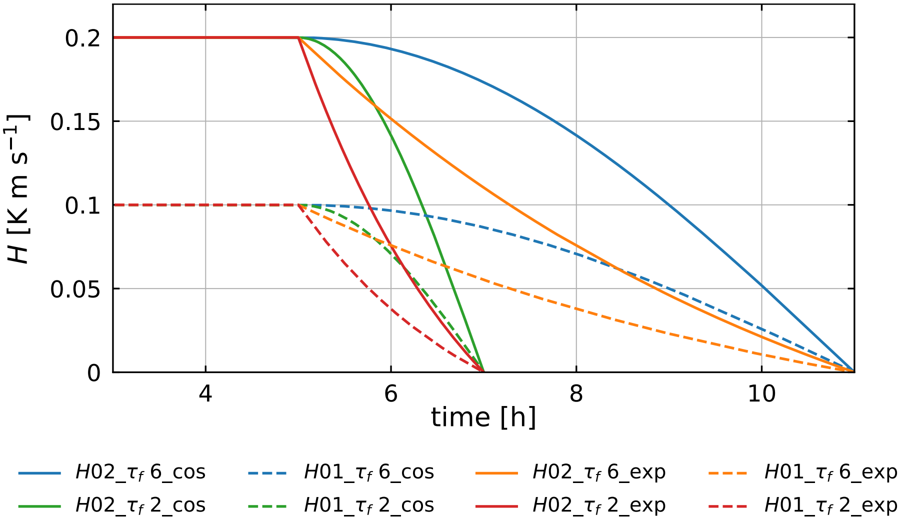

Fig. 1 Time series of the prescribed surface kinematic heat flux. Each color represents a given surface heat flux decay-shape: (sinusoidal, τ_f = 6 h) in blue, (exponential, τ_f = 6 h) in orange, (sinusoidal, τ_f = 2 h) in green, and (exponential, τ_f = 2 h) in red. Solid lines and dashed lines represent simulations with H_0 = 0.2 and 0.1 K m s^{-1} respectively

values for the CBL. Starting from the initial time, the surface kinematic heat flux driving the CBL is maintained constant during a 5-h period, with a value (H_0) of either 0.1 or 0.2 K m s^{-1}. These values are representative for fair-weather conditions in the CBL (e.g. André et al. 1978; LeMone et al. 2000; Lothon et al. 2014). After the 5-h period, the surface kinematic heat flux follows a sinusoidal or an exponential decay-shape during a 2-h or 6-h period τ_f, as visualized in Fig. 1a. By varying the prescribed parameters (H_0, τ_f, λ) and the decay function, we end up with sixteen scenarios for the free-convection simulations. Both modeling and observational studies support a sinusoidal decay of the surface heat flux (Nadeau et al. 2011; Lothon et al. 2014). In this idealized study, we also consider an exponential decay as could occur in the presence of clouds for example, in order to emphasize the new velocity scale for very contrasting surface heat flux decay-shapes. While observations suggest that τ_f = 6 h is a common value for the duration between the maximum and zero surface heat flux, τ_f = 2 h can be considered as a lower-bound value (Lothon et al. 2014, Fig. 8). The analytical expressions for the prescribed decaying surface heat flux are as in E23:

$$H(t) = H_0 \, cos\left(\frac{\pi}{2}\,\frac{t-18000}{3600\tau_f}\right), \text{ or } H(t) = H_0\left(\frac{e^{-\left(\frac{t-18000}{3600\tau_f}\right)}-1}{1-e^{-1}}+1\right), \quad (1a,b)$$

with $t \in$ [18000 s, 25200 s] or [18000 s, 39600 s]. Figure 1 summarizes the time series of the surface kinematic heat flux for the sixteen performed free-convection simulations.

After revealing the new velocity scale from the free-convection simulations, we additionally carry out forced-convection simulations driven by an imposed background wind in the x-direction, with values of either 5 or 15 m s^{-1}. The only purpose of the imposed background wind is to test the sensitivity of the proposed scaling for the bulk of the CBL to the presence of shear-generated turbulence in the simplest configuration, without taking into account Coriolis effects, baroclinicity, or time-varying large-scale flow in the free atmosphere. Hence, the background wind is initialized by a uniform wind-speed profile which is let to freely evolve in the absence of a large scale pressure-gradient. In this context, the domain vertical extent is large enough for preserving a constant wind speed in the free atmosphere during the simulation period, despite the deepening of the boundary layer. For these forced-convection simulations, $(H_0, \tau_f, \lambda) = (0.1\ \mathrm{K\ m\ s^{-1}}, 2\ \text{or}\ 6\,\mathrm{h}, 3\ \mathrm{K\ km^{-1}})$, and the decay-shape is either sinusoidal or exponential, resulting in four scenarios for each background wind velocity. A summary of the runs carried out in this study is given in Table 1.

The domain size for all simulations is 12.8 km in the horizontal directions. In the cases where $H_0 = 0.1\ \mathrm{K\ m\ s^{-1}}$, the domain height is chosen as 4000 m and 3000 m for the experiments with $\tau_f = 6$ h and 2 h, respectively. For all the cases where $H_0 = 0.2\ \mathrm{K\ m\ s^{-1}}$, the domain height is set to 5500 m. The vertical (horizontal) domain-extent is at least two (five) times larger than the maximum boundary-layer height, which is about 2500 m. These proportions are sufficient for sampling several eddies in the simulation domain, and let them evolve independently of the periodic sidewall effects when the surface heat flux is stationary (e.g. Schmidt and Schumann 1989; de Roode et al. 2004), or non-stationary (e.g. Blay-Carreras et al. 2014; Cuchiara and Rappenglück 2017). Following the recommendation of Sullivan et al. (1998), we define the CBL depth as the height of the capping inversion, where the vertical gradient of the mean potential temperature reaches its maximum value. This definition was found to be more appropriate than the definition based on the height of the minimum heat flux, for the use of $\widetilde{r}$ in characterizing the departure from mixed-layer similarity (E23). The grid spacing is 25 m in all three directions. Sensitivity tests for the free-convection simulations have shown that the results are unchanged if the grid spacing is reduced to 12.5 m (E23). One might reasonably assume that results from the forced-convection simulations would also be unchanged for 12.5-m the grid spacing, because our study focuses only on the bulk of the CBL, not the near-surface or entrainment regions. The time step is calculated by the model after each time integration based on stability criteria and varies between 1.2 and 13.5 s across the scenarios.

As turbulence in this study is statistically homogeneous in the x and y directions, we rely on averaging over horizontal cross-sections for estimating the average turbulence statistics. To further improve the convergence of the horizontal-average estimate, we perform time averaging over 1-min intervals. In simulating statistically non-stationary turbulence, the time-averaging length should remain shorter than the eddy turnover time. This requirement is fulfilled in this study because the minimum eddy turnover time across all the simulations is 9.5 min, so the time-dependent eddy turnover time remains at least $\approx$ 10 times larger than the 1-min averaging time selected. In the following, the horizontal and time-averaged statistics are indicated by an overbar, while a prime indicates the turbulent fluctuation around the horizontal and time-average.

The numerical configuration of this LES study, including domain-extent, grid spacing, boundary conditions, model initialization, spin-up time, and turbulence-statistics estimates is validated by the consistency of our scaling results with current understanding of the quasi-equilibrium scaling in the CBL (i.e. when $\widetilde{r} >> 1$), as shown in the following results section. In addition, the ratio of the subgrid-scale and the total turbulence kinetic energy away from the surface (above the first 5–7 grid points) remains smaller than 10%, both during the quasi-equilibrium regime and the out-of-equilibrium regime for all free-convection and forced-convection simulations (not shown). After equilibrium breakdown, we assume that the LES configuration of this study works well, given that the most energetic eddies are resolved.

Table 1 Summary of the runs carried out in this study

Run	Initial surface heat flux, H_0 (K m s^{-1})	Afternoon transition duration, τ_f (h)	Surface heat flux decay shape	Free-atmospheric lapse rate, λ (K km^{-1})	Background wind speed, U (m s^{-1})
$H02\_\tau_f 6\_cos\_\lambda 3$	0.2	6	cos	3	–
$H02\_\tau_f 6\_cos\_\lambda 6$	0.2	6	cos	6	–
$H01\_\tau_f 6\_cos\_\lambda 3$	0.1	6	cos	3	–
$H01\_\tau_f 6\_cos\_\lambda 6$	0.1	6	cos	6	–
$H02\_\tau_f 6\_exp\_\lambda 3$	0.2	6	exp	3	–
$H02\_\tau_f 6\_exp\_\lambda 6$	0.2	6	exp	6	–
$H01\_\tau_f 6\_exp\_\lambda 3$	0.1	6	exp	3	–
$H01\_\tau_f 6\_exp\_\lambda 6$	0.1	6	exp	6	–
$H02\_\tau_f 2\_cos\_\lambda 3$	0.2	2	cos	3	–
$H02\_\tau_f 2\_cos\_\lambda 6$	0.2	2	cos	6	–
$H01\_\tau_f 2\_cos\_\lambda 3$	0.1	2	cos	3	–
$H01\_\tau_f 2\_cos\_\lambda 6$	0.1	2	cos	6	–
$H02\_\tau_f 2\_exp\_\lambda 3$	0.2	2	exp	3	–
$H02\_\tau_f 2\_exp\_\lambda 6$	0.2	2	exp	6	–
$H01\_\tau_f 2\_exp\_\lambda 3$	0.1	2	exp	3	–
$H01\_\tau_f 2\_exp\_\lambda 6$	0.1	2	exp	6	–
$H01\_\tau_f 6\_cos\_\lambda 3\_U5$	0.1	6	cos	3	5
$H01\_\tau_f 6\_exp\_\lambda 3\_U5$	0.1	6	exp	3	5
$H01\_\tau_f 2\_cos\_\lambda 3\_U5$	0.1	2	cos	3	5
$H01\_\tau_f 2\_exp\_\lambda 6\_U5$	0.1	2	exp	3	5
$H01\_\tau_f 6\_cos\_\lambda 3\_U15$	0.1	6	cos	3	15
$H01\_\tau_f 6\_exp\_\lambda 3\_U15$	0.1	6	exp	3	15
$H01\_\tau_f 2\_cos\_\lambda 3\_U15$	0.1	2	cos	3	15
$H01\_\tau_f 2\_exp\_\lambda 6\_U15$	0.1	2	exp	3	15

3 Results

3.1 Evidence from LES Experiments for the New Velocity Scale

When the surface heat flux is constant or varies slowly compared to the convective eddy turnover time, several field experiments, laboratory, and numerical studies emphasized the relevance of w_* for scaling the vertical-velocity variance in the bulk of the CBL, between the approximate height-levels of $0.1z_i$ and $0.8z_i$ (e.g. Willis and Deardorff 1974; Kaimal et al. 1976; Moeng and Sullivan 1994; Fedorovich et al. 1996; Lenschow et al. 2012; Salesky et al. 2017). Motivated by the need for comparing the normalized σ_w^2-profiles between different experiments, a few studies proposed empirical fits (Lenschow et al. 1980; Holtslag and Moeng 1991). Hereafter, we consider the commonly-used fit proposed by Lenschow et al. (1980) (hereafter L80) (e.g. Berg et al. 2017; Zhou et al. 2019; Dewani et al. 2023):

$$\frac{\sigma_w^2}{w_*^2} = 1.8\left(\frac{z}{z_i}\right)^{2/3}\left(1 - 0.8\frac{z}{z_i}\right)^2. \tag{2}$$

Our LES results in Fig. 2a show that during the early afternoon transition when the surface heat flux decays slowly compared to the convective eddy turnover time (i.e. $\widetilde{r} >> 1$), σ_w^2/w_*^2 is a constant on the order of 1, indicating that σ_w^2 is in quasi-equilibrium with the surface heat flux, in line with previous work. Furthermore, Fig. 2b shows that σ_w^2/w_*^2 divided by the L80 fit is approximately 1, indicating that the height-dependence of σ_w^2/w_*^2 is well described by the L80 fit.

During the late afternoon transition when the surface heat flux starts decaying moderately compared to the convective eddy turnover time (i.e. $\widetilde{r} \sim 1$) and later on when the surface heat flux decays rapidly (i.e. $\widetilde{r} << 1$), E23 suggested that σ_w^2 might yet be characterized by the actual w_*, despite the breakdown of the quasi-equilibrium state. The new result that was not discussed in E23 is that σ_w^2/w_*^2 seems to scale with $\widetilde{r}^{\,-1/2}$ during the very late afternoon transition when the surface heat flux decays rapidly compared to the convective eddy turnover time (Fig. 2a), i.e.,

$$\frac{\sigma_w^2}{w_*^2} \propto \widetilde{r}^{\,-1/2} \quad \text{when} \quad \widetilde{r} << 1. \tag{3}$$

In Eq. 3 and hereafter in this study, the symbol $\propto$ indicates only proportionality, with the corresponding coefficient (C) being on the order of 1 (e.g., $1/5 \le C \le 5$ following Tennekes and Lumley (1972)). We emphasize that using the symbol $\propto$ in itself does not give information about whether or not the proportionality coefficient is height-dependent. In the particular case of Eq. 3, Fig. 2a shows that the proportionality coefficient is dependent on height. The approximate $\widetilde{r}$-value of 0.1 is a reasonable estimate for the threshold from where the scaling starts to apply, and the smallest $\widetilde{r}$-value reached in this study is about 10^{-5} (Fig. 2a). For all the LES runs, it takes 6 ± 2 min physical time for $\widetilde{r}$ to decrease from 0.1 to 10^{-5}. We note a transitional state between the end of the regime $\widetilde{r} >> 1$ and the start of the regime $\widetilde{r} << 1$ (see Fig. 2a). However, the investigation of this transitional state is left for future research.

As both quantities σ_w^2/w_*^2 (on the vertical axis) and $\widetilde{r}$ (on the horizontal axis) in Fig. 2a include the parameter w_*, we check for possible self-correlation hidden in Eq. 3. To this end, we replace w_* and $\widetilde{r}$ in Eq. 3 by their definitions. The simplified result reads:

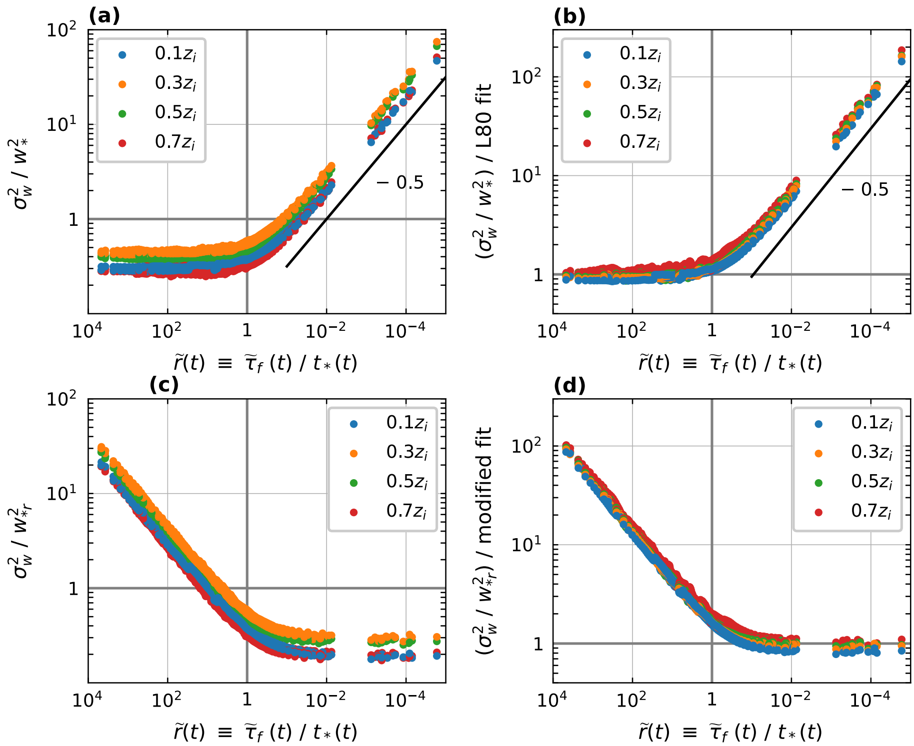

Fig. 2 Results from all free-convection simulations. All subplots show the normalized σ_w^2 at four heights of $0.1z_i$, $0.3z_i$, $0.5z_i$, and $0.7z_i$, as a function of the parameter $\widetilde{r}$. **a** σ_w^2 normalized with w_*. **b** σ_w^2 normalized with w_* and further divided by the L80 fit to remove height dependence when $\widetilde{r} >> 1$. **c** σ_w^2 normalized with w_{*r}. **d** σ_w^2 normalized with w_{*r} and further divided by the modified fit to remove height dependence when $\widetilde{r} << 1$. The modified fit is introduced hereafter in Sect. 3.2

$$\sigma_w^2 \propto \left(\frac{g}{\overline{\theta}} \left| \frac{dH}{dt} \right| z_i^2 \right)^{1/2} \quad \text{when} \quad \widetilde{r} << 1. \tag{4}$$

Eq. 4 indicates that when $\widetilde{r} << 1$, σ_w^2 normalized by $(g/\overline{\theta})|dH/dt|z_i^2)^{1/2}$ is a constant on the order of 1. This result leads us to define the new velocity scale $w_{*r} \equiv ((g/\overline{\theta})|dH/dt|z_i^2)^{1/4}$, the subscript "$r$" indicating the surface heat flux varying rapidly compared to the convective eddy turnover time. Figure 2c shows that σ_w^2/w_{*r}^2 is on the order of 1 for $\widetilde{r}$ in the range $10^{-5} \lesssim \widetilde{r} \lesssim 0.1$. Similarly to Eq. 3, the proportionality coefficient in Eq. 4 is dependent on height (Fig. 2c).

According to Eq. 4, the distinct empirical σ_w^2-scaling revealed in Fig. 2c explicitly includes the surface heat flux decay-rate, not its magnitude. This situation is unusual as it differs from the well-known quasi-equilibrium regime where H is the relevant parameter for scaling σ_w^2. To get more physical insights into the relevance of H and dH/dt when $\widetilde{r} >> 1$ and $\widetilde{r} << 1$ respectively, we first analyze the situation where the surface heat flux varies slowly compared to the eddy turnover time ($\widetilde{r} >> 1$). As the forcing time scale $\widetilde{\tau}_f \equiv |H^{-1}dH/dt|^{-1}$ is defined based on the time change of the surface heat flux *relative* to its actual magnitude, the surface heat flux time change can be neglected compared to its magnitude for durations much smaller

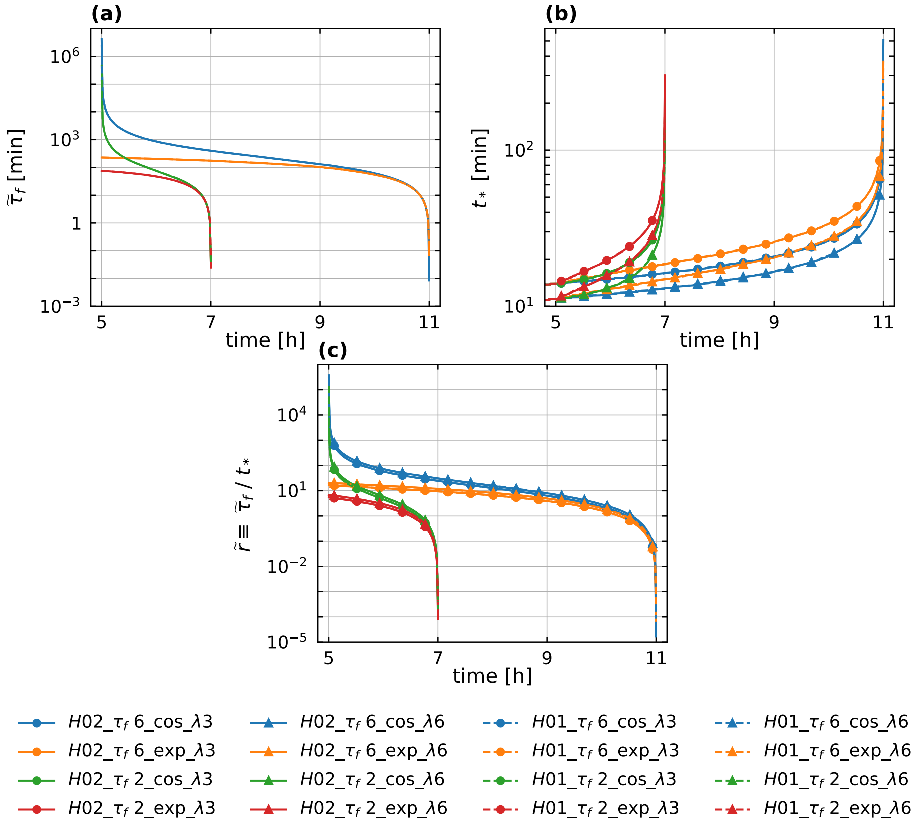

Fig. 3 Time series of the characteristic time scale of the surface heat flux decay (**a**), the eddy turnover time (**b**), and the parameter $\widetilde{r}$ (**c**). Each color represents a given surface heat flux decay-shape: (sinusoidal, $\tau_f = 6$ h) in blue, (exponential, $\tau_f = 6$ h) in orange, (sinusoidal, $\tau_f = 2$ h) in green, and (exponential, $\tau_f = 2$ h) in red. Solid lines and dashed lines represent simulations with $H_0 = 0.2$ and 0.1 K m s^{-1} respectively. Circles and triangles represent simulations with $\lambda = 3$ and 6 K km^{-1}, respectively. The prescribed surface kinematic heat fluxes in this study are independent of the free-atmospheric lapse rates, and so are $\widetilde{\tau}_f \equiv |H^{-1}dH/dt|^{-1}$. Thus, the legend can be applied to panel (**a**) by omitting the symbols

than $\widetilde{\tau}_f$, but it can no longer be neglected for durations on the order of $\widetilde{\tau}_f$. Thus, when $\widetilde{r} >> 1$, the surface heat flux time change is negligible compared to its magnitude for a time duration on the order of the eddy turnover time, and the actual heat flux magnitude is physically representative for the forcing driving the strength of the vertical-velocity fluctuations over that duration. As a result of decreasing $\widetilde{\tau}_f$ and increasing t_* during the afternoon transition (Fig. 3a, b), the parameter $\widetilde{r} \equiv |H^{-1}dH/dt|^{-1}/t_*$ decreases (Fig. 3c). When $\widetilde{r} << 1$, σ_w^2 can no longer keep pace with the small and rapidly decaying H on the one hand, while the time change of H is much larger than H itself on the other hand (as reflected by very small $\widetilde{\tau}_f$ in Fig. 3a). Hence, it is physically plausible to use dH/dt rather than H in order to scale σ_w^2.

Equation 4 suggests that the important parameters for describing σ_w^2 during the out-of-equilibrium regime $\widetilde{r} << 1$ are $g/\overline{\theta}$, dH/dt, and z_i. This seemingly suggests that the initial state of the out-of-equilibrium process does not constrain the similarity at all subsequent time moments. However, this is not the case. Actually, the surface heat flux magnitude at the initial state of the regime $\widetilde{r} << 1$ is an implicit defining parameter of the similarity characterized by the proposed velocity scale w_{*r}, within the specific similarity framework considered in this study. Indeed, for given $g/\overline{\theta}$, dH/dt, and z_i during the regime $\widetilde{r} << 1$, which starts when $\widetilde{r} \approx 0.1$, the definition of $\widetilde{r}$ ($\widetilde{r} \equiv |H^{-1}dH/dt|^{-1}/t_* = H^{4/3}|dH/dt|^{-1}(g/\overline{\theta})^{1/3}z_i^{-2/3}$) constrains the surface heat flux magnitude at the initial state when $\widetilde{r} \approx 0.1$, so that $0.1 = H_{0.1}^{4/3}|dH/dt|_{0.1}^{-1}(g/\overline{\theta})_{0.1}^{1/3}z_{i0.1}^{-2/3}$ where the subscript 0.1 indicates values at the initial time when $\widetilde{r} \approx 0.1$. This constraint by the initial surface heat flux magnitude distinguishes the out-of-equilibrium regime ($\widetilde{r} << 1$) from the equilibrium regime ($\widetilde{r} >> 1$) where σ_w^2 is only dependent on the actual parameters ($g/\overline{\theta}$, H, z_i). Also, the out-of-equilibrium regime in the particular setups of our study is preceded by the quasi-equilibrium regime of a fully-developed CBL driven by surface heating (the importance of this additional implicit hypothesis is shown in Sect. 3.4). Due to this limitation, we can not infer results for rapidly increasing surface heat flux during the morning transition, because this stage of the diurnal cycle is preceded by a stable regime. During the evening transition stage when the surface heat flux becomes negative, Blay-Carreras et al. (2014) reported counter-gradient heat flux observations from the BLLAST campaign, that is a delay period of about 30 to 80 min when the surface heat flux becomes negative while the near surface potential temperature gradient remains positive. As the proposed scaling in our study applies during the very late afternoon stage when the surface heat flux is still positive, further research efforts are required to understand how the counter-gradient heat flux phase can benefit from the proposed scaling.

3.2 Height-Dependence of σ_w^2/w_{*r}^2 in the Regime $\widetilde{r} << 1$

Using observations from the Air Mass Transformation experiment (Lenschow and Agee 1976), Lenschow et al. (1980) proposed a reference fit (Eq. 2) for describing the height-dependence of σ_w^2/w_*^2 in the context of quasi-equilibrium between σ_w^2 and the surface heat

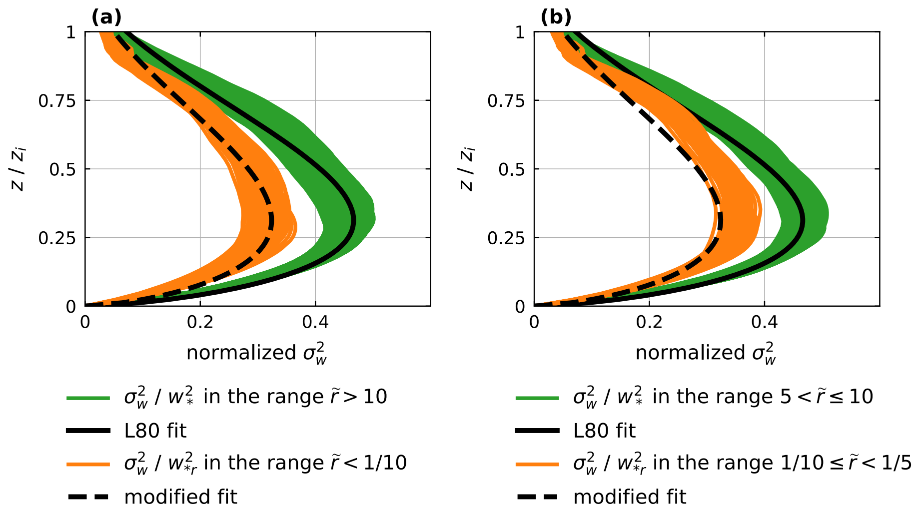

Fig. 4 Results from all free-convection simulations. **a** σ_w^2 normalized with w_* when $\widetilde{r} > 10$ (green curves), and σ_w^2 normalized with w_{*r} when $\widetilde{r} < 1/10$ (orange curves). The L80 fit is given by Eq. 2, while the modified fit refers to replacing the factor 1.8 in the right-hand-side of Eq. 2 by 1.25. **b** σ_w^2 normalized with w_* when $5 < \widetilde{r} \leq 10$ (green curves), and σ_w^2 normalized with w_{*r} when $1/10 \leq \widetilde{r} < 1/5$ (orange curves)

flux. Elguernaoui et al. (2023) showed that such quasi-equilibrium prevails when $\widetilde{r} >> 1$. To find out whether or not the right-hand side of Eq. 2 might also apply for describing the height-dependence of σ_w^2/w_{*r}^2 in the regime $\widetilde{r} << 1$, we first need to select approximate empirical threshold-values of $\widetilde{r}$ for characterizing the bounds of the regimes $\widetilde{r} >> 1$ and $\widetilde{r} << 1$. The respective threshold-values of 10 and 1/10 seem reasonable according to Fig. 2a, c showing σ_w^2/w_*^2 and σ_w^2/w_{*r}^2 respectively at the selected normalized altitudes of 0.1, 0.3, 0.5, and $0.7z_i$. Figure 4a confirms that the L80 fit is a good approximation for σ_w^2/w_*^2 in the range $\widetilde{r} > 10$. Actually, the L80 fit is still a good approximation for σ_w^2/w_*^2 in the range $5 < \widetilde{r} \leq 10$ (Fig. 4b), suggesting that the quasi-equilibrium regime $\widetilde{r} >> 1$ prevails for values of $\widetilde{r}$ as small as 5. Figure 4a, b shows that the magnitude of σ_w^2/w_{*r}^2 in the range $1/10 \leq \widetilde{r} < 1/5$ is consistently larger than in the range $\widetilde{r} < 1/10$, suggesting that the new regime $\widetilde{r} << 1$ is not yet reached for $\widetilde{r} > 1/10$. We emphasize that we do not aim to provide a thorough quantitative analysis for the threshold-values characterizing the bounds of the regimes $\widetilde{r} >> 1$ and $\widetilde{r} << 1$.

Based on our LES results in Fig. 4a, the L80 fit is not appropriate for describing the σ_w^2/w_{*r}^2-profiles when $\widetilde{r} << 1$, because the magnitude of σ_w^2/w_*^2-profiles when $\widetilde{r} >> 1$ is distinctly larger than the magnitude of σ_w^2/w_{*r}^2-profiles. Despite this quantitative gap due to a scaling-regime change, the σ_w^2/w_{*r}^2-profiles remain qualitatively similar to the σ_w^2/w_*^2-profiles, suggesting that the σ_w^2/w_{*r}^2-profiles could be described by a modified fit similar to the L80 fit. Replacing the scaling factor 1.8 in the right-hand-side of Eq. 2 by an empirical value of 1.25 based on our LES data leads to a modified fit which reasonably describes the height variations of σ_w^2/w_{*r}^2. Our study does not aim to determine the "best fit" for σ_w^2/w_{*r}^2, but simply to propose an adequate fit for collapsing σ_w^2/w_{*r}^2 from different heights when $\widetilde{r} << 1$ in Fig. 2c. The modified fit is good enough for this purpose, as suggested by Fig. 2d.

3.3 The Effect of Background Wind

In the presence of background wind in the CBL, and within a quasi-equilibrium framework relating the turbulent vertical-velocity fluctuations to the surface heat flux, w_* remains useful for characterizing σ_w^2 in the bulk of the CBL to a first approximation, i.e. the friction velocity u_* can be ignored, provided that the stability parameter $-z_i/L = k(w_*/u_*)^3$ (L is the Obukhov length, and $k \approx 0.4$ is the von Kármán constant) exceeds the approximate range of 5–10 (Moeng and Sullivan 1994; Wyngaard 2010). This condition is satisfied in all forced-convection simulations of our study for $\widetilde{r} >> 1$ (Fig. 5), so w_*^2 is a good scaling parameter for σ_w^2 in the bulk of the CBL (Fig. 6a). Furthermore, Fig. 6a shows that σ_w^2/w_*^2 slightly decreases with increasing wind speed (or decreasing $-z_i/L$ magnitude, see Fig. 5), in line with the results from Salesky et al. (2017). This aspect is also illustrated in Fig. 7a showing σ_w^2/w_*^2-profiles for $\widetilde{r} > 10$, and for different background wind speeds.

Interestingly, when $\widetilde{r} << 1$, Fig. 6a, b suggests that the new scaling results (i.e., Eq. 3) obtained from the free-convection simulations seems to remain valid for the forced-convection simulations, highlighting the robustness of the new scaling. This finding further motivates us to examine the physical basis of the new scaling. Note that the modified fit deduced from the free-convection simulations when $\widetilde{r} < 1/10$, applies also for the forced-convection simulations irrespective of the wind-speed magnitude (Fig. 7b).

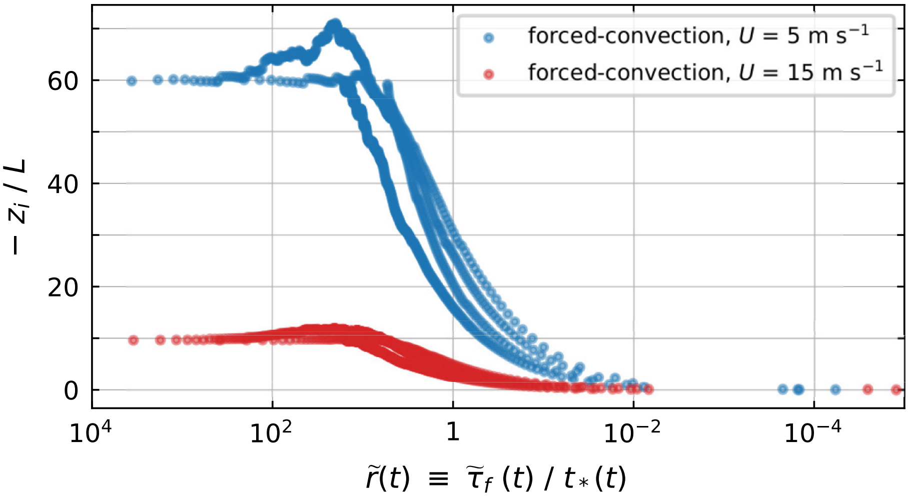

Fig. 5 Results from all forced-convection simulations. The stability parameter $-z_i/L$ as a function of the parameter $\tilde{r}$

3.4 Scaling Arguments from the Budget-Equation of the Vertical Turbulent Heat Flux Supporting the New Velocity Scale

For a more detailed investigation of the physical processes supporting the relevance of w_* and w_{*r}, we turn to the budget-equation of the vertical turbulent heat flux. Using the Boussinesq approximation for the dry CBL, assuming statistical homogeneity in the horizontal directions, and no subsidence, the equation reads (e.g. Wyngaard 2010):

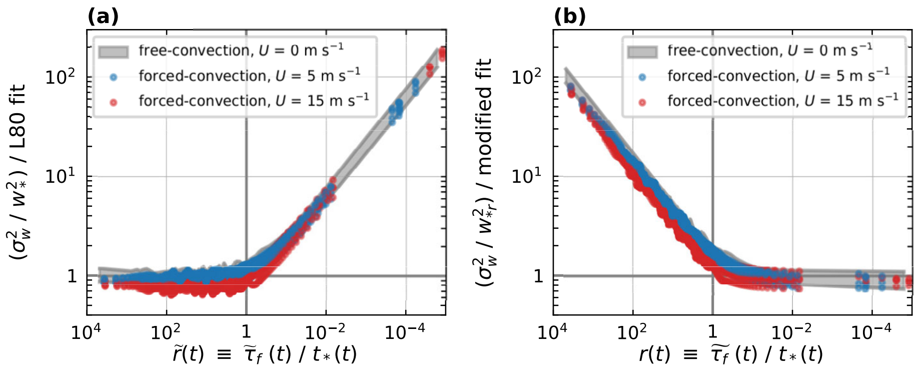

Fig. 6 Results from all free-convection, and all forced-convection simulations. Both subplots show the normalized σ_w^2 at four heights of $0.1z_i$, $0.3z_i$, $0.5z_i$, and $0.7z_i$, as a function of the parameter $\tilde{r}$. **a** σ_w^2 normalized with w_*, and further divided by the L80 fit to remove height variability when $\tilde{r} >> 1$. **b** σ_w^2 normalized with w_{*r}, and further divided by the modified fit to remove height dependence when $\tilde{r} << 1$. The gray shading encapsulate the results for all free convection simulations shown in Fig. 2b, d

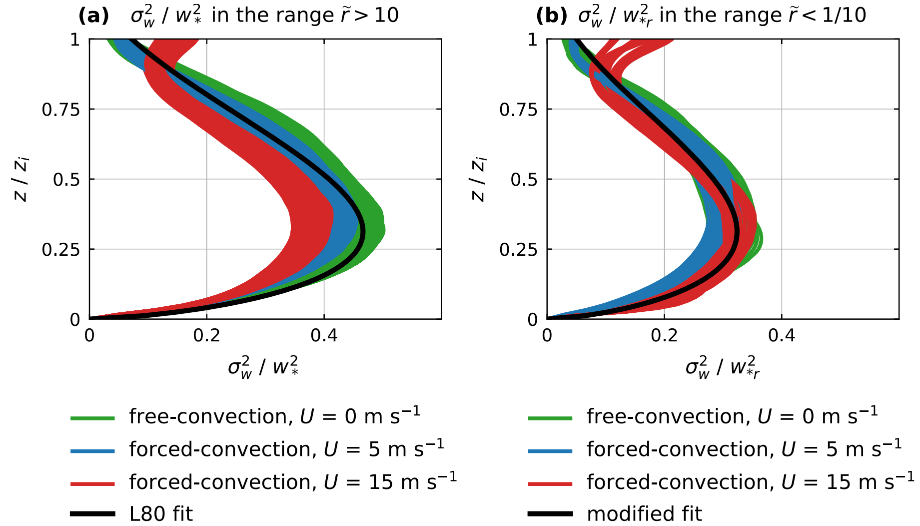

Fig. 7 Results from all free-convection, and all forced-convection simulations. **a** σ_w^2 normalized with w_* when $\widetilde{r} > 10$. **b** σ_w^2 normalized with w_{*r} when $\widetilde{r} < 1/10$. The L80 fit is given by Eq. 2, while the modified fit refers to replacing the factor 1.8 in the right-hand-side of Eq. 2 by 1.25

$$\frac{\partial \overline{w'\theta'}}{\partial t} = \sigma_\theta^2 \frac{g}{\overline{\theta}} - \frac{1}{\rho_0}\overline{\theta' \frac{\partial p'}{\partial z}} - \sigma_w^2 \frac{\partial \overline{\theta}}{\partial z} - \frac{\partial \overline{w'w'\theta'}}{\partial z} + \alpha \overline{w' \frac{\partial^2 \theta'}{\partial x_j \partial x_j}} + \nu \overline{\theta' \frac{\partial^2 w'}{\partial x_j \partial x_j}}, \quad (5)$$

where α and ν are the thermal diffusivity and kinematic viscosity. The terms are the turbulent heat flux tendency, the buoyancy production, the pressure-gradient interaction, the mean-gradient production, the turbulent transport, and the molecular terms. Using Eq. 5, we aim to develop the scaling for σ_w^2 during (i) the initial quasi-equilibrium regime characterized by a slow decay of the surface heat flux compared to the convective eddy turnover time, then (ii) the out-of-equilibrium regime where the surface heat flux decays rapidly compared to the convective eddy turnover time.

Using LES for day 33 of the Wangara experiment, Deardorff (1974) and André et al. (1978) analyzed the balance in Eq. 5 for the bulk of the CBL. They found that the heat flux tendency is negligible during a few hours around midday, the leading term is the buoyancy production, which is mainly balanced by the pressure term acting as a sink for the turbulent heat flux through all the bulk of the CBL. Lenschow et al. (1980) confirmed these results with an observational study. The mean-gradient production and the turbulent transport are on the same order of magnitude of, but smaller than the buoyancy production through most of the bulk of the CBL, except within a height interval of approximately $0.2{-}0.4z_i$ where these terms change sign. Finally, it is known that when the heat flux tendency is negligible, the leading terms in Eq. 5 are on the order of $\theta_* w_*^2/z_i$ where $\theta_* \equiv H/w_*$ (Deardorff 1974; André et al. 1978; Lenschow et al. 1980).

Using our LES data from the free-convection simulations, we calculated the heat flux tendency, the buoyancy production, the mean-gradient production, and the turbulent transport. As the molecular terms as well as the subgrid scale terms arising from the LES approximation of Eq. 5 can be safely neglected within the bulk of the CBL, the residual term (i.e. heat flux tendency—buoyancy production—mean-gradient production—turbulent transport)

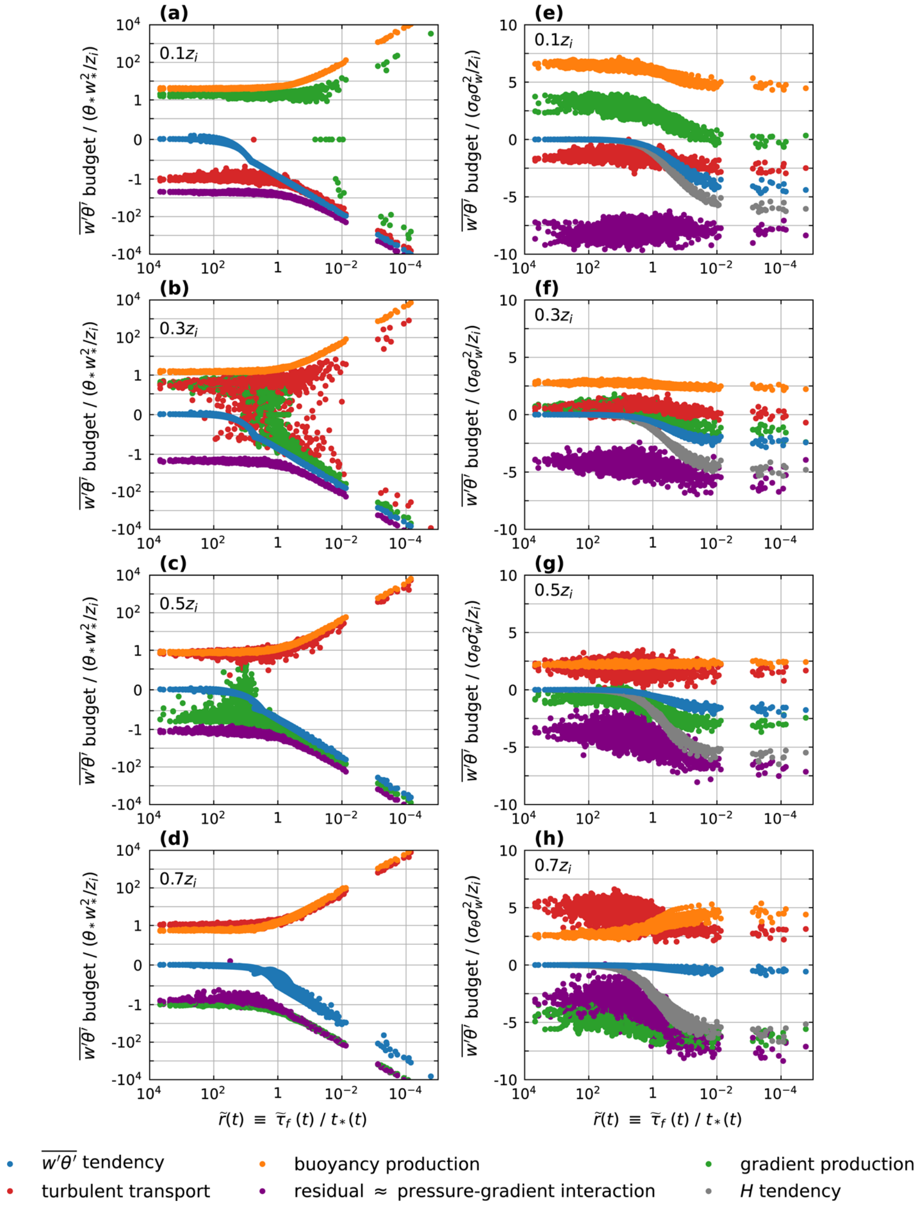

Fig. 8 Results from all the free-convection simulations. **a**–**d** $\overline{w'\theta'}$ budget normalized by $\theta_* w_*^2/z_i$ as a function of $\widetilde{r}$, at four heights of $0.1z_i$, $0.3z_i$, $0.5z_i$, and $0.7z_i$. **e**–**h**, $\overline{w'\theta'}$ budget normalized by $\sigma_\theta \sigma_w^2/z_i$ as a function of $\widetilde{r}$, at four heights of $0.1z_i$, $0.3z_i$, $0.5z_i$, and $0.7z_i$. The gray dots indicate the surface heat flux tendency (dH/dt)

represents essentially the pressure-gradient interaction. This indirect estimate of the pressure-gradient interaction term is consistent with previous LES studies (Deardorff 1974; André et al. 1978) where this term was calculated directly (see Fig. 10 in the Appendix). Figure 8a–d shows the results for the turbulent heat flux budget normalized with $\theta_* w_*^2/z_i$ at heights

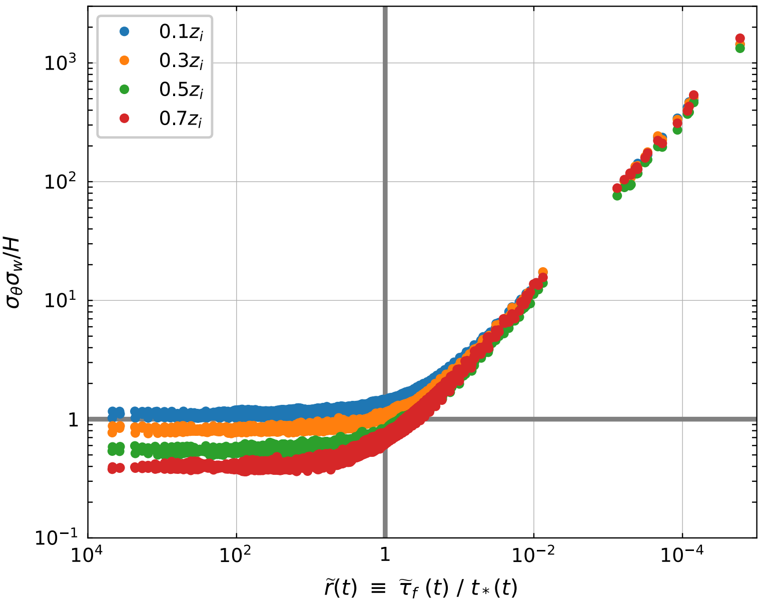

Fig. 9 Results from all free-convection simulations. The product of the vertical-velocity and potential temperature standard deviation at four heights of $0.1z_i$, $0.3z_i$, $0.5z_i$, normalized by the surface heat flux, as a function of $\widetilde{r}$

of $0.1z_i$, $0.3z_i$, $0.5z_i$, and $0.7z_i$. A thorough analysis of the vertical variations of the budget terms is out of the scope of this study. Nevertheless, we illustrate the normalized profiles from quasi-steady state conditions in the Appendix to further emphasize the agreement of our results with previous studies. Figure 8a–d has two main aims, validating the LES results during quasi-steady state, and illustrating the utility of the parameter $\widetilde{r}$ for characterizing the departure from quasi-steady state. When the heat flux tendency is negligible, the leading source/sink terms scale with $\theta_* w_*^2/z_i$, consistent with the current understanding (Deardorff 1974; André et al. 1978; Lenschow et al. 1980). Furthermore, this quasi-steady state scaling occurs when $\widetilde{r} >> 1$, and a departure is observed when $\widetilde{r}$ becomes on the order of 1.

The scales w_* and w_{*r} can be deduced from the heat flux budget as follows. When $\widetilde{r} >> 1$, $\overline{w'\theta'}$ is mainly produced by the buoyancy term, $\sigma_\theta^2 g/\overline{\theta}$, which scales with $\sigma_\theta \sigma_w^2/z_i$ according to Wyngaard (2010) (see also Fig. 8e–h). Then,

$$\sigma_w^2 \propto \sigma_\theta \frac{g}{\overline{\theta}} z_i . \tag{6}$$

Combining Eq. 6 with the following,

$$\sigma_\theta \sigma_w \propto H, \tag{7}$$

reflecting the quasi-equilibrium adjustment of the temperature and vertical-velocity fluctuations in the bulk of the CBL to the surface heat flux changes (see Fig. 9), we find that $\sigma_w \propto \left(g/\overline{\theta} H z_i\right)^{1/3}$, namely, σ_w scales with the convective velocity scale.

When $\widetilde{r} << 1$, Fig. 8e–h shows that the balance in Eq. 5 remains largely unchanged, except for the heat flux tendency which now becomes on the same order of magnitude as the leading budget-terms, away from the region affected by entrainment (Fig. 8h). Then we can write,

$$\frac{\partial \overline{w'\theta'}}{\partial t} \propto \sigma_\theta^2 \frac{g}{\overline{\theta}} . \tag{8}$$

Table 2 Summary of the scaling steps/assumptions for deriving the velocity scales w_* and w_{*r} depending on whether $\widetilde{r} >> 1$ or $\widetilde{r} << 1$, based on the $\overline{w'\theta'}$ budget

Assumptions	$\widetilde{r} >> 1$	$\widetilde{r} << 1$
$\sigma_\theta^2 \frac{g}{\overline{\theta}} \propto \frac{\sigma_\theta \sigma_w^2}{z_i}$ (equivalent to Eq. 6)	Valid	Valid
$\sigma_\theta \sigma_w \propto H$ (Eq. 7)	Valid	Not valid
$\frac{\partial \overline{w'\theta'}}{\partial t} \propto \sigma_\theta^2 \frac{g}{\overline{\theta}}$ (Eq. 8)	–	Valid
$\frac{\partial \overline{w'\theta'}}{\partial t} \propto \frac{dH}{dt}$ (Eq. 9)	–	Valid

Furthermore, scaling the leading terms with $\sigma_\theta \sigma_w^2/z_i$ remains valid when $\widetilde{r} << 1$ compared to when $\widetilde{r} >> 1$ (Fig. 8e–h), and thus Eq. 6 remains valid. This emphasizes the particular physical setup of this study where the quasi-equilibrium regime of the CBL constitutes the initial conditions for the following out-of-equilibrium regime. Indeed, the leading budget-terms scale with $\sigma_\theta \sigma_w^2/z_i$ when $\widetilde{r} << 1$ because this scaling already prevailed when $\widetilde{r} >> 1$ (Fig. 8e–h). In a hypothetical setup where the regime $\widetilde{r} << 1$ does not originate from the regime $\widetilde{r} >> 1$, our LES setup may not enable us to conclude whether or not the leading budget-terms scale with $\sigma_\theta \sigma_w^2/z_i$.

However, the quasi-equilibrium adjustment of the temperature and vertical-velocity fluctuations in the bulk of the CBL to the surface heat flux changes does not apply in the regime $\widetilde{r} << 1$ as result of rapidly varying surface heat flux (Fig. 9). Then Eq. 7 is no longer valid. Combining Eqs. 6 and 8 to eliminate σ_θ, then noting from Fig. 8e–g that the heat flux tendency in the bulk of the CBL is on the same order of magnitude as the surface heat flux tendency, i.e,

$$\frac{\partial \overline{w'\theta'}}{\partial t} \propto \frac{dH}{dt}, \tag{9}$$

we find $\sigma_w \propto ((g/\overline{\theta})|dH/dt|z_i^2)^{1/4}$, namely, the new convective velocity scale as deduced from the LES experiments (Eq. 4). A summary of the scaling steps for both cases ($\widetilde{r} >> 1$ and $\widetilde{r} << 1$) is given in Table 2.

4 Conclusion and Discussion

The quasi-equilibrium assumption results in the well-known convective velocity scale (w_*) for the CBL, as long as the surface heat flux (H) varies over time scales longer than the convective eddy turnover time, i.e. $\widetilde{r} \equiv \widetilde{\tau}_f/t_* \equiv |H^{-1}dH/dt|^{-1}/t_* >> 1$. In this study, we revisited this result for the regime where the surface heat flux decays over time scales shorter than the convective eddy turnover time, i.e. $\widetilde{r} << 1$, assuming that the out-of-equilibrium regime proceeds from a breakdown of the quasi-equilibrium regime.

In a first step, the empirical LES results demonstrate that the vertical-velocity variance scales with $w_{*r} \equiv ((g/\overline{\theta})|dH/dt|z_i^2)^{1/4}$, when $\widetilde{r} << 1$. Indeed, we found that σ_w^2/w_{*r}^2 is a constant on the order of 1 in the range $10^{-5} \lesssim \widetilde{r} \lesssim 0.1$. This result holds also in the presence of background wind, as suggested by additional simulations of forced convection. Even though the new velocity scale does not depend on the concurrent surface heat flux magnitude during the out-of-equilibrium regime $\widetilde{r} << 1$, the proposed scaling framework is constrained by the surface heat flux magnitude at the initial stage of the regime $\widetilde{r} << 1$ (when $\widetilde{r} \approx 0.1$) through the definition of the parameter $\widetilde{r}$.

In a second step, we provided physical arguments supporting the new velocity scale based on a scaling analysis of the budget-equation of the vertical turbulent heat flux using the LES data. Based on existing knowledge where (i) the leading terms in the $\overline{w'\theta'}$ budget scale with $\sigma_\theta \sigma_w^2/z_i$, and (ii) $\sigma_\theta \sigma_w$ scales with H reflecting the quasi-equilibrium adjustment of the the potential temperature/vertical velocity fluctuations in the bulk of the CBL to the surface heat flux changes, we derived the convective velocity scale w_* when $\widetilde{r} >> 1$. Moving from the regime $\widetilde{r} >> 1$ to the regime $\widetilde{r} << 1$, the scaling $\sigma_\theta \sigma_w \propto H$ breaks down. Furthermore, the main balance between the source/sink terms in the $\overline{w'\theta'}$ budget remains valid, and these terms still scale with $\sigma_\theta \sigma_w^2/z_i$. The important change in the budget is that the heat flux tendency becomes on the same order of magnitude as the leading terms. Using this new information together with the approximation $\partial \overline{w'\theta'}/\partial t \propto dH/dt$, we derived the new velocity scale w_{*r}.

Let us emphasize that within the specific setups of this study, $|dH/dt|$ does not increase to infinitely large values toward the end of the regime $\widetilde{r} << 1$ which is marked by the time when H becomes zero. This remark does not contradict the statement of "rapidly decaying surface heat flux", by which we mean that the characteristic time scale of the surface heat flux decay is much shorter than the convective eddy turnover time (i.e. $\widetilde{r} << 1$), and by which we do not necessarily imply that $|dH/dt|$ becomes arbitrarily large. Indeed, because $\widetilde{r} \equiv \widetilde{\tau}_f/t_* \equiv |H^{-1}dH/dt|^{-1}/t_* = H^{4/3}|dH/dt|^{-1}(g/\overline{\theta})^{1/3}z_i^{-2/3}$, a very small H can make the parameter $\widetilde{r}$ very small, without requiring an infinitely large $|dH/dt|$. Hence, our study does not permit us to infer results in cases where the surface heat flux decay-rate increases to infinity. In addition, the out-of-equilibrium regime in this study is preceded by the well-known quasi-equilibrium regime of a fully-developed CBL driven by surface heating. Thus, our study does not permit us to infer results in cases where the out-of-equilibrium regime of interest is not preceded by a quasi-equilibrium regime. These are important limitations of this study. Further research is needed to understand which part of our results can be generalized to other non-stationary configurations.

In this study, we considered the scaling of the vertical-velocity variance but not the variance of the longitudinal and lateral velocity components. The reason is that the proposed scaling arguments based on the budget-equation of the vertical turbulent heat flux apply to the kinetic energy of the vertical velocity fluctuations. Eventually, one might expect a kinetic energy transfer from the vertical to the horizontal velocity components through pressure redistribution, as it is case in the quasi-equilibrium CBL. The scaling of the longitudinal and lateral velocity components in the case of the out-of-equilibrium CBL is constrained by understanding the return to isotropy in the out-of-equilibrium CBL, which is left for future studies. As TKE is defined as the sum of the horizontal and vertical velocity variances divided by two, investigating the scaling for the horizontal-velocity variances, combined with the proposed scaling in this study, would benefit for scaling TKE in the out-of-equilibrium CBL. The scaling of other turbulence statistics, such as the variance of potential temperature or humidity, could also eventually benefit from the scaling ideas proposed for the vertical-velocity variance in this study.

Appendix 1: Profiles of the $\overline{w'\theta'}$ Budget Terms During Quasi-Steady State Conditions

Figure 10 shows that our LES results for the profiles of the $\overline{w'\theta'}$ budget terms during quasi-steady state conditions are in line with previous LES studies (Deardorff 1974; André et al. 1978).

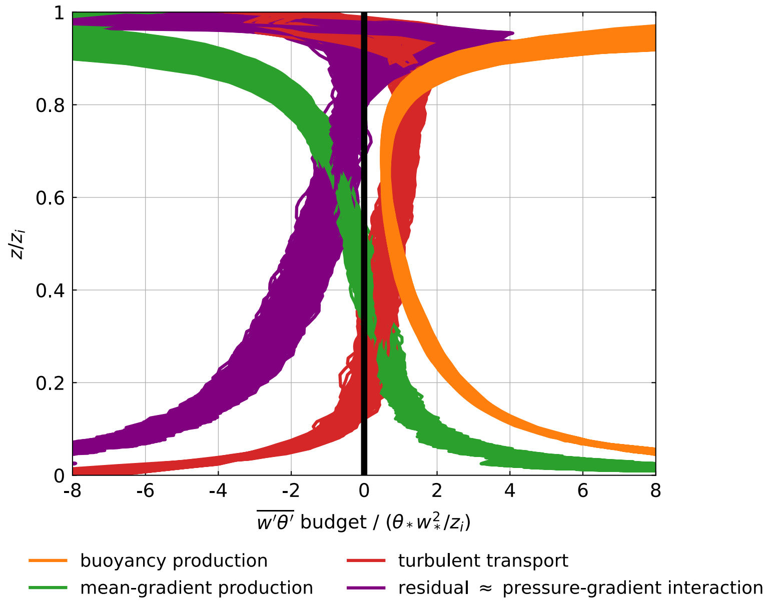

Fig. 10 Results from all free-convection simulations. Profiles of the $\overline{w'\theta'}$-budget terms when $\widetilde{r} > 10$, i.e. quasi-steady state conditions when the $\overline{w'\theta'}$ tendency is negligible compared to the leading source/sink terms

Acknowledgements Dan Li acknowledges support from U.S. National Science Foundation (NSF) under the Award number AGS-1853354 and also support from the Alexander von Humboldt Foundation. We thank the three reviewers for their thorough comments which helped improve the manuscript. The computations were performed on resources provided by Sigma2-the National Infrastructure for High Performance Computing and Data Storage in Norway, Grant No. NN9506k.

Funding Open access funding provided by University of Bergen (incl Haukeland University Hospital)

Declarations

Conflict of interest The authors declare that they have no Conflict of interest.

References

André JC, Moor GD, Lacarrère P, du Vachat R (1978) Modeling the 24-hour evolution of the mean and turbulent structures of the planetary boundary layer. J Atmos Sci 35:1861–1883

Berg LK, Newsom RK, Turner DD (2017) Year-long vertical velocity statistics derived from doppler lidar data for the continental convective boundary layer. J Appl Meteorol Clim 56(9):2441–2454

Blay-Carreras E, Pardyjak ER, Pino D, Alexander DC, Lohou F, Lothon M (2014) Countergradient heat flux observations during the evening transition period. Atmos Chem Phys 14(17):9077–9085

Blay-Carreras E, Pino D, Vilà-Guerau de Arellano J, van de Boer A, De Coster O, Darbieu C, Hartogensis O, Lohou F, Lothon M, Pietersen H (2014) Role of the residual layer and large-scale subsidence on the development and evolution of the convective boundary layer. Atmos Chem Phys 14(9):4515–4530

Cuchiara GC, Rappenglück B (2017) Single-column model and large eddy simulation of the evening transition in the planetary boundary layer. Environ Fluid Mech 17:777–798

Deardorff JW (1970) Convective velocity and temperature scales for the unstable planetary boundary layer and for Rayleigh convection. J Atmos Sci 27:1211–1213

Deardorff JW (1974) Three-dimensional numerical study of turbulence in an entraining mixed layer. Boundary-Layer Meteorol 7:199–226

Deardorff JW (1980) Stratocumulus-capped mixed layers derived from a three-dimensional model. Boundary-Layer Meteorol 18:495–527

Dewani N, Sakradzija M, Schlemmer L, Leinweber R, Schmidli J (2023) Dependency of vertical velocity variance on meteorological conditions in the convective boundary layer. Atmos Chem Phys 23(7):4045–4058

de Roode SR, Duynkerke PG, Jonker HJJ (2004) Large-eddy simulation: how large is large enough? J Atmos Sci 61:403–421

Elguernaoui O, Reuder J, Li D, Maronga B, Bakhoday Paskyabi M, Wolf T, Esau I (2023) The departure from mixed-layer similarity during the afternoon decay of turbulence in the free-convective boundary layer: results from large-eddy simulations. Boundary-Layer Meteorol 188:259–284

Fedorovich E, Kaiser R, Rau M, Plate E (1996) Wind tunnel study of turbulent flow structure in the convective boundary layer capped by a temperature inversion. J Atmos Sci 53:1273–1289

Garratt JR (1994) The Atmospheric Boundary Layer. Cambridge University Press, Cambridge

Holtslag AAM, Moeng CH (1991) Eddy diffusivity and countergradient transport in the convective atmospheric boundary layer. J Atmos Sci 48:1690–1698

Kaimal JC, Wyngaard JC, Haugen DA, Coté OR, Izumi Y, Caughey SJ, Readings CJ (1976) Turbulence structure in the convective boundary layer. J Atmos Sci 33:2152–2169

LeMone MA, Grossman RL, Coulter RL, Wesley ML, Klazura GE, PouIos GS, Blumen W, Lundquist JK, Cuenca RH, Kelly SF, Brandes EA, Oncley SP, McMillen RT, Hicks BB (2000) Land-atmosphere interaction research, early results, and opportunities in the walnut river watershed in southeast kansas: Cases and able. Bull Am Meteorol Soc 81(4):757–780

Lenschow DH, Agee EM (1976) Preliminary results from the air mass transformation experiment (AMTEX). Bull Am Meteorol Soc 57(11):1346–1355

Lenschow DH, Wyngaard JC, Pennell WT (1980) Mean-field and second-moment budgets in a baroclinic, convective boundary layer. J Atmos Sci 37:1313–1326

Lenschow DH, Lothon M, Mayor SD, Sullivan PP, Canut G (2012) A comparison of higher-order vertical velocity moments in the convective boundary layer from lidar with in situ measurements and large-eddy simulation. Boundary-Layer Meteorol 143:107–123

Lothon M, Lohou F, Pino D, Couvreux F, Pardyjak ER, Reuder J, Vilà-Guerau de Arellano J, Durand P, Hartogensis O, Legain D, Augustin P, Gioli B, Lenschow DH, Faloona I, Yagüe C, Alexander DC, Angevine WM, Bargain E, Barrié J, Bazile E, Bezombes Y, Blay-Carreras E, van de Boer A, Boichard JL, Bourdon A, Butet A, Campistron B, de Coster O, Cuxart J, Dabas A, Darbieu C, Deboudt K, Delbarre H, Derrien S, Flament P, Fourmentin M, Garai A, Gibert F, Graf A, Groebner J, Guichard F, Jiménez MA, Jonassen M, Van den Kroonenberg A, Magliulo V, Martin S, Martinez D, Mastrorillo L, Moene AF, Molinos F, Moulin E, Pietersen HP, Piguet B, Pique E, Román-Cascón C, Rufin-Soler C, Saïd F, Sastre-Marugán M, Seity Y, Steeneveld GJ, Toscano P, Traullé O, Tzanos D, Wacker S, Wildmann N, Zaldei A (2014) The BLLAST field experiment: boundary-layer late afternoon and sunset turbulence. Atmos Chem Phys 14:10,931–10,960

Maronga B, Gryschka M, Heinze R, Hoffmann F, Kanani-Sühring F, Keck M, Ketelsen K, Letzel MO, Sühring M, Raasch S (2015) The parallelized large-eddy simulation model (palm) version 4.0 for atmospheric and oceanic flows: model formulation, recent developments, and future perspectives. Geosci Model Dev 8:2515–2551

Moeng CH, Sullivan PP (1994) A comparison of shear- and buoyancy-driven planetary boundary layer flows. J Atmos Sci 51:999–1022

Nadeau DF, Pardyjak ER, Higgins CW, Fernando HJS, Parlange MB (2011) A simple model for the afternoon and early evening decay of convective turbulence over different land surfaces. Boundary-Layer Meteorol 141:301–324

Nicholls S, Lemone MA (1980) The fair weather boundary layer in gate: The relationship of subcloud fluxes and structure to the distribution and enhancement of cumulus clouds. JAS 37(9):2051–2067

Piacsek SA, Williams GP (1970) Conservation properties of convection difference schemes. J Comput Phys 6:392–405

Salesky ST, Chamecki M, Bou-Zeid E (2017) On the nature of the transition between roll and cellular organization in the convective boundary layer. Boundary-Layer Meteorol 163:41–68
Schmidt H, Schumann U (1989) Coherent structure of the convective boundary layer derived from large-eddy simulations. J Fluid Mech 200:511–562
Stull RB (1988) An Introduction to Boundary Layer Meteorology. Kluwer Academic Publishers, Dordrecht
Sullivan PP, Moeng C, Stevens B, Lenschow DH, Mayor SD (1998) Structure of the entrainment zone capping the convective atmospheric boundary layer. J Atmos Sci 55:3042–3064
Tennekes H, Lumley JL (1972) A first Course in Turbulence. MIT Press, Cambridge
Williamson JH (1980) Low-storage Runge–Kutta schemes. J Comput Phys 35:48–56
Willis GE, Deardorff JW (1974) A laboratory model of the unstable planetary boundary layer. J Atmos Sci 31:1297–1307
Wyngaard JC (1973) On surface-layer turbulence. In: Haugen DA (ed) Workshop on Micrometeorology. American Meteorological Society, Boston, pp 101–149
Wyngaard JC (2010) Turbulence in the Atmosphere. Cambridge University Press, Cambridge
Zhou B, Sun S, Sun J, Zhu K (2019) The universality of the normalized vertical velocity variance in contrast to the horizontal velocity variance in the convective boundary layer. J Atmos Sci 76(5):1437–1456